Journal of Catalysis 259 (2008) 17–25

Contents lists available at ScienceDirect

Journal of Catalysis

www.elsevier.com/locate/jcat

The mechanism of propene oxidation to acrolein on iron antimony oxide

Changjun Zhang, C. Richard A. Catlow *

Department of Chemistry, University College London, 20 Gordon Street, London, WC1H 0AJ, United Kingdom

ARTICLE INFO

Article history:
Received 3 April 2008
Revised 14 June 2008
Accepted 17 June 2008
Available online 8 August 2008

Keywords:
Surfaces
Catalysis
DFT

ABSTRACT

Density functional theory is used to investigate the microscopic mechanisms of oxidation of propene (CH_3–CH=CH_2) to acrolein (CH_2=CH–CHO) over iron antimony oxide ($FeSbO_4$). Two routes for acrolein formation are investigated. The first starts from a chemisorbed state, in which propene binds with the surface via the π orbitals; acrolein formation can be triggered first by the abstraction of an allylic H atom towards the active bridging O atom, followed by the abstraction of a second H atom toward either an O or an Sb atom and the subsequent desorption of the acrolein thereby formed. The second route starts from a direct dissociation of the propene molecule without the need to proceed through a chemisorbed precursor, which, however, is kinetically hindered. The first route is compared with the mechanisms proposed from experiment. We also discuss the mechanisms of propane oxidation to acrolein, in which propene oxidation is an important step.

1. Introduction

The partial oxidation of propene (CH_3–CH=CH_2) to acrolein (CH_2=CH–CHO) represents a major use of selective oxidation catalysis in the petrochemical industry [1,2]. Iron antimony oxide ($FeSbO_4$) has been the preferred catalyst for this reaction [3–6]. Despite extensive studies of the reaction over $FeSbO_4$, the reaction mechanism remains elusive. There is general agreement that the reaction proceeds via the Mars–van Krevelen mechanism; that is, propene is oxidized on active centers of the catalyst, and lattice oxygen atoms are incorporated into the acrolein product [1]. However, mechanistic details vary widely. In earlier experiments, Burrington et al. [7] suggested that the rate-determining step is the abstraction of an allylic hydrogen from propene to form a π-allyl species, which is then rapidly converted to acrolein, whereas Aso et al. [8] suggested that one surface oxygen abstracts the allylic hydrogen of a propene molecule, followed by a subsequent addition of another surface oxygen to convert it into acrolein, with the second step being slower. This argument over the rate-determining step is echoed by Keulks et al. [9], who further suggested that after the abstraction of the allylic hydrogen, the addition of oxygen occurs before the abstraction of a second hydrogen. Yet another mechanism proposed by Allen et al. [10] assumes that propene adsorbs in a weakly held state; the first hydrogen abstraction is relatively facile, and the second hydrogen abstraction and the oxygen addition could both be rate-determining, although the sequence of these two steps is unclear. In addition, it also has been suggested that the surface must be in a partially reduced state for acrolein formation [10,11]; however, a more recent study showed that the catalyst needs to be oxidized to achieve maximum activity [12].

Theoretical approaches are being increasingly used as aids in unraveling mechanistic details of surface reactions. Consequently, in the present work, we undertook a density function theory (DFT) study of propene oxidation to acrolein on $FeSbO_4$, with the aim of determining the reaction mechanisms. We note that intense efforts are now underway to use propane instead of propene as a feedstock for the synthesis of acrolein [13–16], due to the greater availability of propane. Thus, identifying the mechanisms of propene oxidation also would be important in understanding propane oxidation, in which the former reaction is involved. Recently, we carried out a DFT study of propane oxidation on $FeSbO_4$ [17]. We identified the so-called *one-stage* reaction route for a direction conversion of propane to acrolein (the desired route in synthesis technology) without having to proceed by (i) an initial dehydrogenation of propane to propene and (ii) a subsequent propene oxidation, which often is referred to as the *two-stage* route [18]. The present study does, however, allow us to comment on the two-stage route, which might compete with the one-stage route, as the dehydrogenation of propane to propene is considered, and a comparable barrier (~1.2 eV) to that in the one-stage route is determined.

This study builds on substantial previous work aimed at gaining insight into the complex crystal structure (see Fig. 1a) and surface chemistry of $FeSbO_4$ [19–23], in which Sb and Fe cations distribute in the octahedral sites within the oxygen lattice and in which the cation distribution has been investigated in recent years. Grau-Crespo et al. [20–22] carried out extensive DFT calculations to show that Sb and Fe cations have a clear preference to alternate

* Corresponding author.
E-mail address: c.r.a.catlow@ucl.ac.uk (C.R.A. Catlow).

0021-9517/$ – see front matter
doi:10.1016/j.jcat.2008.06.027

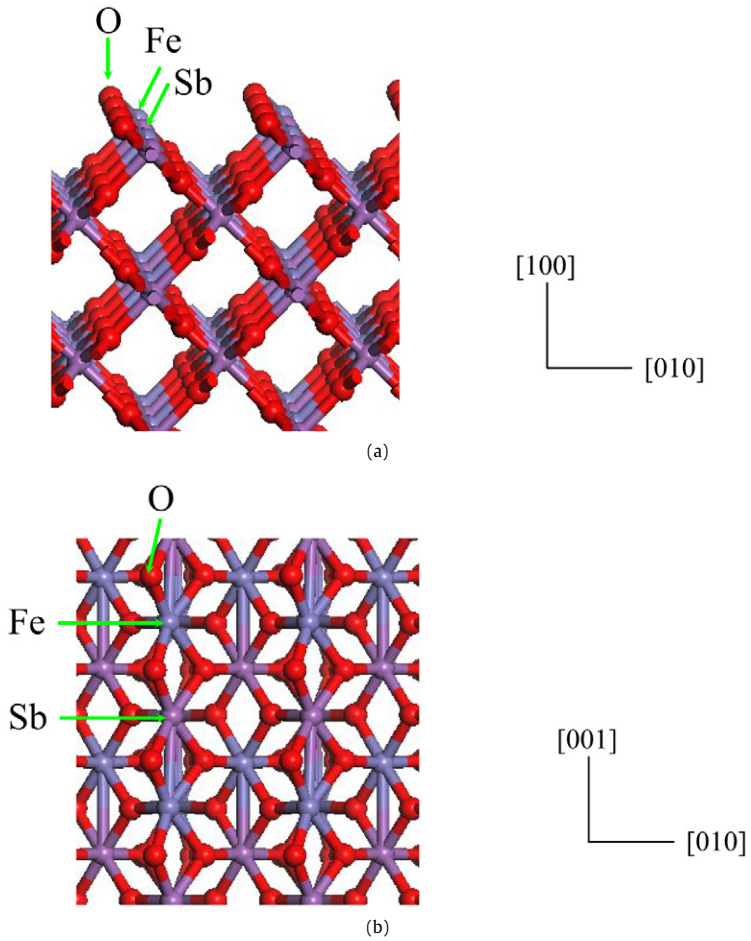

Fig. 1. Top view (a) and side view (b) of the $FeSbO_4(100)$ surface. O atoms are in red, Sb in violet, and Fe in light blue. The [100] direction is perpendicular to the surface plane; the [001] and the [010] directions are along and perpendicular to the bridging O rows, respectively. (For interpretation of the references to color in this figure legend, the reader is referred to the web version of this article.)

along the *c* axis of the crystal, while these chains of alternating cations connect laterally with significant disorder in the *a*–*b* plane, preventing three-dimensional long-range ordering. These findings agree with the corresponding experimental studies [24]. Therefore, in the present study, we built the $FeSbO_4$ surface from the bulk structure established in their work. We chose the $FeSbO_4(100)$ surface that is the most prominent surface in experiment [25], as shown schematically in Fig. 1b.

2. Calculations

All calculations were performed using the Vienna Ab initio Simulation Program (VASP), a widely used plane-wave pseudopotential DFT package [26–29]. The DFT + *U* methodology [30–33] was used in lieu of the commonly used local density (LDA) or generalized-gradient approximation (GGA) method to describe the exchange and correlation terms, because these latter methods are known to fail in the description of the electronic properties of some metal oxides. The DFT + *U* technique combines DFT and a Hubbard Hamiltonian to account for the intra-atomic Coulomb repulsion, which is not well described in standard DFT. In $FeSbO_4$, the DFT + *U* approach has proven essential in obtaining correct electronic and magnetic properties, as shown by Grau-Crespo et al. [22]. The GGA + *U* approximation was used with a GGA functional built from the Perdew and Zunger local functional, with the spin interpolation formula of Vosko et al. and the gradient corrections of Perdew et al. [34–36]. The U_{eff} (i.e., the difference between the spherically averaged Hubbard parameter *U* and the screened exchange energy *I* in the formulation of Dudarev et al. [33]) was set at 4 eV, as recommended by Grau-Crespo et al. [22]. The details of the implementation of the DFT + *U* technique in the VASP code have been given by Rohrbach et al. [37]. In addition, the interaction between the valence electrons and the core was described with the projected augmented wave (PAW) method in the implementation of Kresse and Joubert [38]. The number of plane waves is controlled by a cutoff energy of 500 eV, which is sufficient to obtain well-converged energies.

Our surface model uses a 2×2 unit cell (9.37×12.46 Å^2 surface area), to accommodate the propene molecule. The model also contains nine atomic layers or three layers of $FeSbO_4$ units and ~12 Å vacuum region. Tests showed that these are adequate to obtain satisfactorily converged adsorption energies for propene. The *k*-point spacing used to sample the Brillouin zone was chosen as 0.03 Å^{-1}, which corresponds to a $4 \times 3 \times 1$ *k*-point mesh for the 2×2 unit cell. Another important aspect is the ordering of the Fe^{3+} magnetic moments in the systems. As found by Grau-Crespo et al. [23], the antiferromagnetic ordering of the Fe^{3+} in the $FeSbO_4(100)$ surface, with spins of the diagonal Fe–Fe pair orientating in antiparallel directions, is the same as in the bulk. We have also found this ordering to be the most stable spin configuration in the propene-adsorbed systems. In the calculations of adsorption energies, we report all of the energies with respect to the isolated propene molecule unless stated otherwise.

To investigate the reaction pathway and mechanism, we used the climbing image nudged elastic band (CI-NEB) algorithm [39]. In practice, usually eight images are used between the initial reac-

tants and final products via a linear interpolation, and then optimized with the CI-NBE method to locate the saddle points. Once a candidate transition state is obtained by this procedure, it is then submitted to a vibrational frequency calculation using the finite-differences method. The structure is accepted as a *bona fide* TS if it has one imaginary frequency, as indeed was the case with those structures reported later. Reaction barriers are determined as the energy differences between the saddle points and the starting points of the calculated minimum energy pathway.

3. Results

3.1. Molecular adsorption

We first consider molecular propene on the surface, which can adsorb in many possible configurations. In the most stable adsorbed structure (shown in Fig. 2a), we find that the C=C bond axis of the molecule is almost parallel to the O–Sb bond axis beneath. The C–Sb and the C–O bond distances become 2.23 and 1.46 Å, respectively, and the original C=C bond in the molecule elongates to 1.52 Å, which is close to a typical C–C single bond distance. These geometries clearly indicate that the molecule binds to the O–Sb via its π orbitals. The adsorption is calculated to be significantly exothermic (-1.25 eV). In contrast to the adsorption associated with the O–Sb bond, the adsorption associated with the O–Fe bond is energetically less favorable (exothermic by 0.31 eV). We note that the C–Sb bond formed in the former case is $\sim$0.1 Å shorter than that of the C–Fe bond in the latter case. Given that Sb has a larger radius than Fe, the more favorable adsorption associated with C–Sb bond formation may be ascribed largely to the stronger covalent bonding of the C–Sb. This feature is similar to that in bulk $FeSbO_4$, where the O–Sb bond also has a greater covalent character than the O–Fe bond [21].

The molecule also may bond solely with the bridging O atom (denoted as BO hereafter), without directly involving any metal atoms. An example is shown in Fig. 2b, in which a BO binds to the two C atoms of the double bond and the BO almost breaks bonds with the metal atoms beneath. The O–Sb and the O–Fe distances become 2.4 and 2.8 Å, respectively, whereas they are $\sim$1.94 Å on the pure surface. This adsorption, essentially a propene epoxidation process, is moderately exothermic (-0.29 eV). In contrast, the hydrogen abstraction from the configuration in Fig. 2b, a necessary step in forming acrolein, is endothermic by $>$1.4 eV. The high endothermicity, along with the anticipated barriers in the possible subsequent reactions, suggests that this route for acrolein formation would be energetically prohibitive. Thus, we excluded this configuration from further study. Other possible adsorption modes include those in which the CH or CH_2 species of the molecule bind with a BO; the latter, which is slightly more favorable, is shown in Fig. 2c. But here adsorption is endothermic by $+0.44$ and $+0.29$ eV, respectively, indicating that neither of these adsorption modes is stable.

A further adsorption mode would involve the molecule binding with the BO via its H atoms, an example of which is shown in Fig. 2d. Because of the weak bonding strength between the BO and the H atoms, these configurations have very low adsorption energies (i.e., they are weakly physisorbed). The foregoing results indicate that the configuration in Fig. 2a is clearly the most stable thus adsorbed configuration. We chose this configuration, designated IS_A hereinafter, as the starting configuration in our investigation of the acrolein formation pathways.

3.2. Reaction paths for acrolein formation

We now consider the abstraction of an H atom from propene in IS_A, where the molecule is already attached to an O atom. Because there are six different H atoms in IS_A, as labeled in Fig. 3a (where the top view is shown for the sake of clarity), there are many possibilities for the initial H abstraction, which we examine in turn. We note that the initial abstraction cannot occur on an H_D atom (see the labeling convention in Fig. 3a), because this atom points away from the surface, with no adjacent surface site to accommodate the dissociated H atom. Abstraction of an H_C atom also is difficult and is endothermic by 0.90 eV, because the resulting configuration (Fig. 3b) is much less stable than those configurations resulting from the abstraction of other H atoms, as discussed below.

The abstraction of an H_A or H_B atom by its nearest BO along [010] or [001] would lead to the formation of the configurations shown in Fig. 3c or 3d, respectively. Both processes are exothermic; however, neither is kinetically viable. For the abstraction of H_A, the initial distance between H_A and the nearest BO along [010] is clearly too long (4.6 Å); thus, the C–Sb bond must break so that H_A can orientate to be closer to the BO. However, the resulting configuration after breaking the C–Sb bond (i.e. essentially the same as that in Fig. 2c) is $\sim$1.4 eV higher in energy than the starting configuration. Moreover, it has positive adsorption energy—that is, the adsorbed state is unstable. For the abstraction of H_B, we found a high barrier of 1.86 eV, suggesting that the process is kinetically prohibitive, since H_B is abstracted toward BO along the [001] direction (i.e., along the BO row). But binding with BO along this direction is energetically unfavorable, because the lone pairs of the O atom point toward the [010] direction. Indeed, in the TS, the C–H bond needs to be stretched considerably to 1.63 Å so that the H_B atom can bond with the BO; in the dissociated configuration (Fig. 3d), the H_B atom moves toward a position to which the O lone pair points.

It now becomes evident that in forming acrolein, the reaction will follow the initial abstraction of H_E or H_F (i.e., the allylic H) if starting from IS_A. We discuss the former in detail; results obtained for the latter were similar. We have identified two formation routes, designated paths *I* and *II*, which are illustrated in Figs. 4 and 5. In both, the reaction starts with the abstraction of H_E. The H_E moves towards a neighboring BO, and simultaneously the C–Sb bond elongates; the TS (i.e. TS_I-1) forms when the C–H and the C–Sb distances are 1.45 and 2.47 Å, respectively. The barrier to this process is 1.10 eV. We note that in the dissociated state (DS_I-1), the C–Sb bond is already broken due to the formation of a new C=C bond; the molecule binds to the surface via the O–C (i.e. the C in a CH_2 species) bond, implying that the other CH_2 and the CH species of the molecule can readily orientate without significantly reducing the stability of the molecule. Indeed, we found two such configurations (DS_I-2 and DS_{II}-2 in Figs. 4 and 5, respectively) that have almost the same energies as that of DS_I-1. The CI-NEB calculations show negligible barriers in transforming DS_I-1 to either DS_I-2 or DS_{II}-2. Following DS_I-2 (i.e., path *I* in Fig. 4), an H atom dissociates toward an adjacent O along [010]. TS_I-2 forms when the C–H and the O–H distances are 1.38 and 1.34 Å, respectively. In the resulting configuration, the CH_2CHCHO entity lies upright on the surface, binding only weakly to the metal atoms (at O–Sb and O–Fe distances of 2.81 and 2.32 Å, respectively). Only 0.12 eV of energy is required to desorb the resulting acrolein.

In contrast, following DS_{II}-2 (i.e., path *II* in Fig. 5), an H atom dissociates toward an adjacent Sb atom. The TS (TS_{II}-2) forms when the C–H and the Sb–H distances are 1.50 and 2.03 Å, respectively. The CH_2CHCHO molecule also binds weakly to the metal atoms (with O–Sb and O–Fe distances of 2.26 and 2.42 Å, respectively). An energy of 0.31 eV is required for the molecule to desorb. From our calculations, the abstraction of the second H atom in path *I* (with a barrier of 1.27 eV) is slightly less favorable than that in path *II* (with a barrier of 1.13 eV). This finding is somewhat surprising, because the former abstraction is more exothermic than

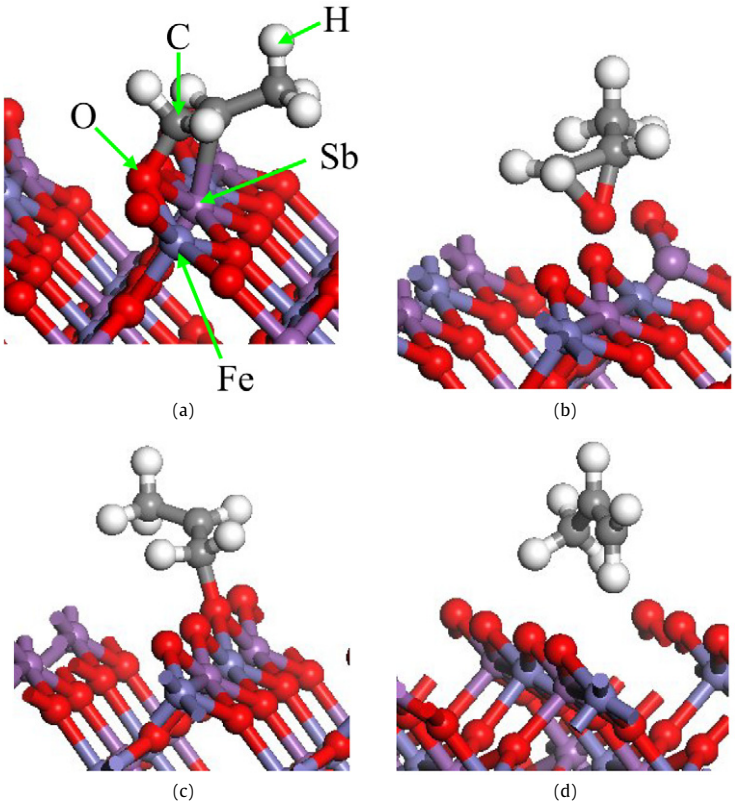

Fig. 2. Various propene adsorbed configurations.

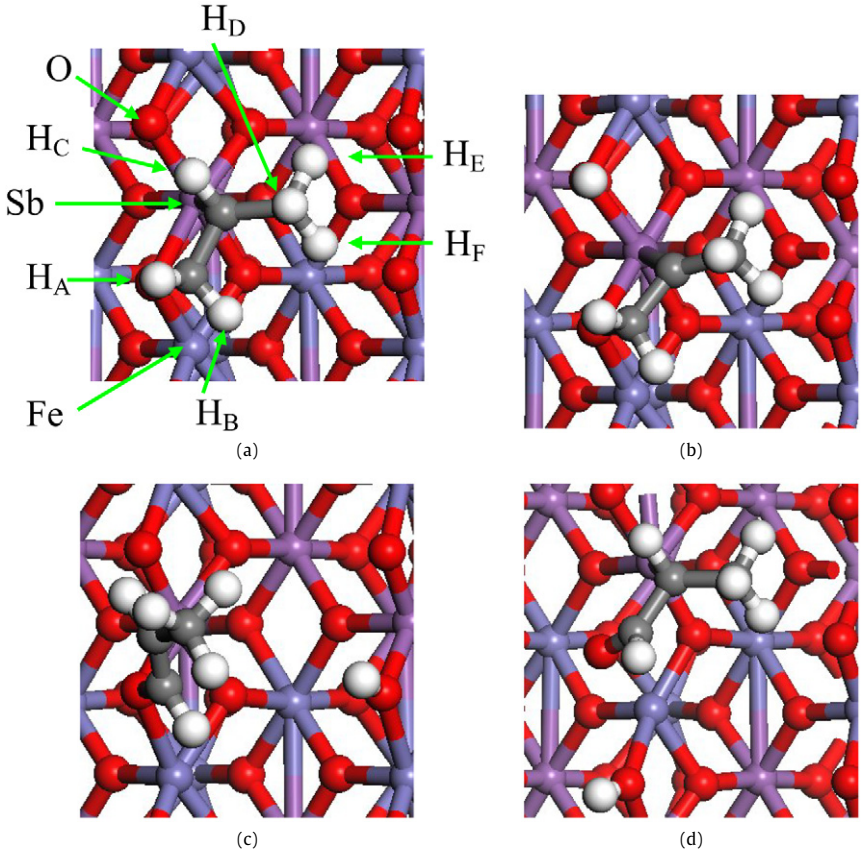

Fig. 3. (a) Top view of the most stable molecular adsorption state, with labeled H atoms. (b, c, and d) Top views of the resulting configurations upon dissociations of H_C, H_A, and H_B atoms.

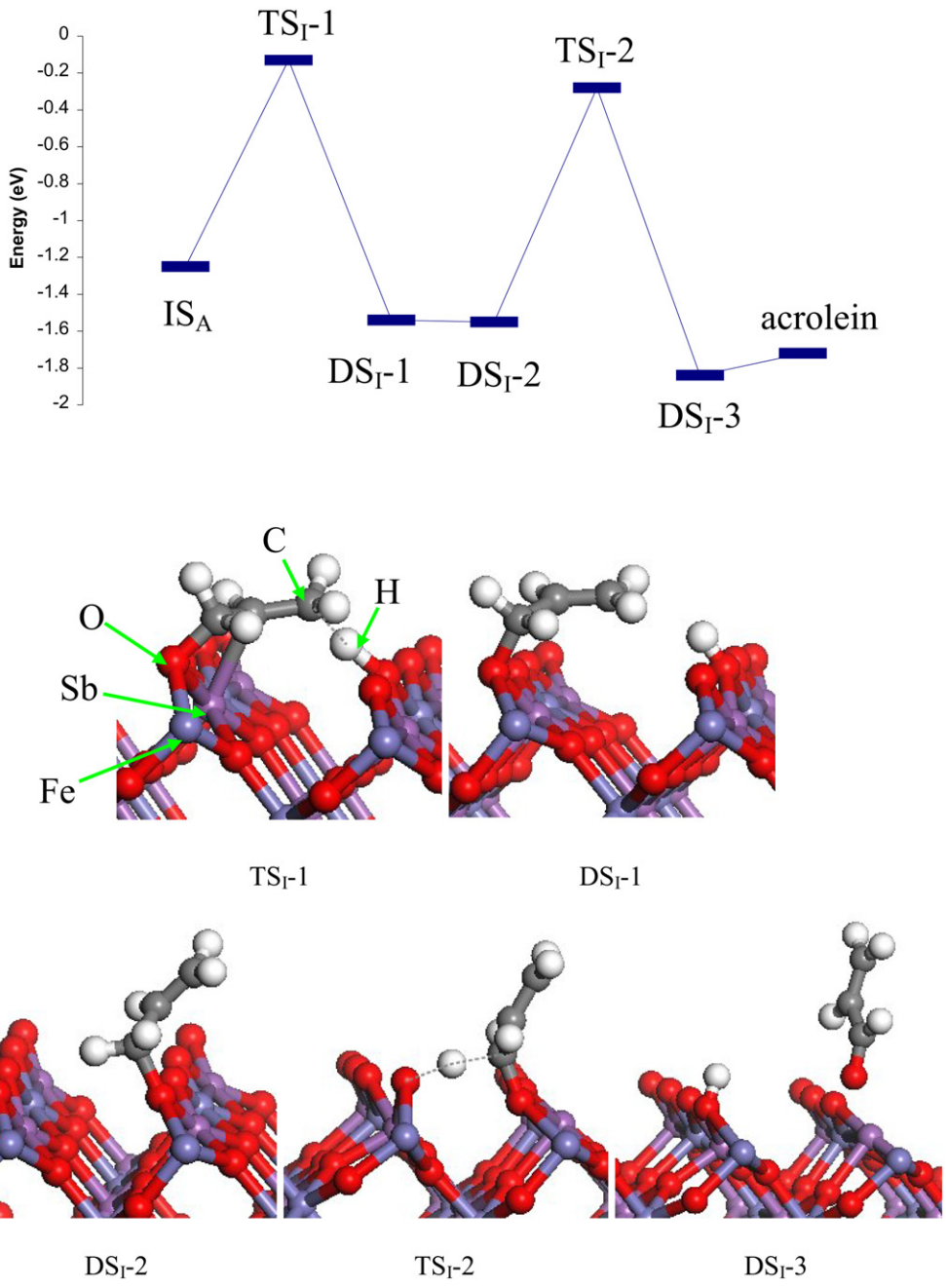

Fig. 4. Energy profile of path *I* for acrolein formation. The energy zero refers to the isolated systems (IS_A) in which propene is initially not in close contact with the surface, e.g. configuration *d* in Fig. 2.

the latter. However, a close examination of the TS structures reveals that in the TS_I-2 of path *I*, the BO moves significantly along [010] (by ∼0.6 Å) and [100] (by ∼0.3 Å) from its original location to bond with the dissociating H_E. This movement results in significantly weakened O–metal bonds. On the other hand, in TS_{II}-2 of path *II*, the displacement of the Sb atom is relatively small, because of the much larger H–Sb bond distance (1.73 Å) compared with the H-O bond distance. The difference can be attributed to the greater accessibility to the dissociating H atom of the outmost 5*p* orbital of the Sb compared with the O 2*p* orbital, so that in bonding with the dissociating H, the Sb does not have to move toward the H atom as much as it does toward the O atom. Indeed, the H–Sb distance in TS_{II}-2 is significantly longer than the H–O distance in TS_I-2. Finally, we note that near the end of path *II*, the H, bonded with the Sb, could move further to bond with an adjacent BO; however, this process has a barrier of 0.92 eV, larger than the energy required to desorb the acrolein molecule. Thus, H movement is less likely than the direct desorption of acrolein from structure DS_{II}-3.

For reactions of the type described above to proceed, the barrier height should not exceed the initial binding energy of the molecule, calculated as 1.25 eV. But this criterion is not fulfilled by, for example, path *I*, suggesting that propene can desorb before the reaction occurs. Therefore, we also examined those possible reaction pathways in which the propene molecule is not initially chemisorbed on the surface (e.g., configuration *d* in Fig. 2, designated IS_A). Again, we consider first the abstraction of H, because the addition of an O atom to the molecule at this stage is unlikely. (In that case, a structure similar to that in Fig. 2b would form, from which the subsequent reaction would be prohibitive.) There

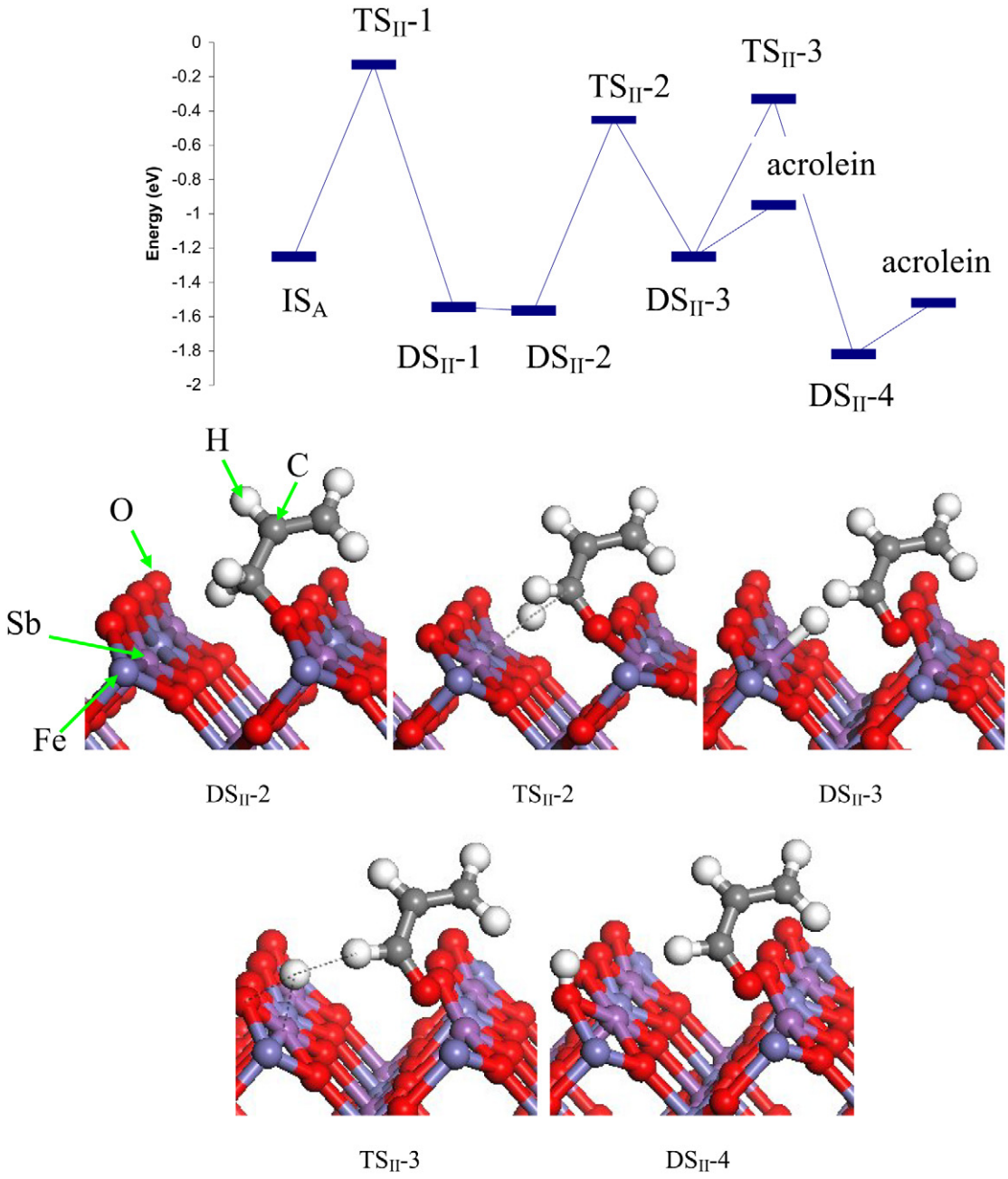

Fig. 5. Energy profile of path *II* for acrolein formation. The energy zero is the same as that in Fig. 4. The first H abstraction is the same as that in path *I*, and thus the configurations of IS_A, TS_{II}-1, and DS_{II}-1 are the same as those shown in Fig. 4. Note that the process from DS_{II}-3 to DS_{II}-4 has a large barrier, and thus the desorption of acrolein from DS_{II}-3 is preferred.

are two different mechanisms for the initial abstraction of H—heterolytic splitting and homolytic splitting—and thus two different pathways for acrolein formation. In the former case, an H atom in propene dissociates to a BO, and the remaining entity forms a C–Sb bond with the surface. (The pathway resulting in the C–Fe bond formation is energetically less favorable and thus is not considered.) In the latter case, the splitting occurs solely on O atoms, without the direct involvement of any metal atoms.

Considering first the reaction, which starts with heterolytic splitting (i.e. path *III* in Fig. 6), the dissociation of an allylic hydrogen occurs, along with O–H and C–Sb bond formation. In the TS (i.e., TS_{III}-1), the C–H, O–H, and C–Sb distances are 1.39, 1.33, and 2.60 Å, respectively, and the energy barrier is 1.01 eV. Following the first step, a second H atom is abstracted toward another BO; the TS (i.e. TS_{III}-2) forms when the C–H bond stretches to 1.44 Å. This process is endothermic by 0.8 eV and has a barrier of 1.27 eV. In the resulting configuration (DS_{III}-2), the CH_2 species doubly bonds with the CH species in the middle of the molecule; consequently, the CH–CH bond (with a distance of 1.41 Å) in the molecule is similar to a single bond. To complete its tetravalency, the CH species (associated with the Sb) needs a double-bond character with the Sb, also demonstrated by a relatively short C–Sb bond distance (2.10 Å). But the double bond can occur only at the expense of a weakening of the O–Sb bonds; an average ~0.1 Å increase in the O–Sb bond lengths is calculated compared with those in the initial configuration, possibly accounting for the endothermicity seen in this step of the reaction. The third step is the addition of a BO to the CH_2CHCH entity, leading to the for-

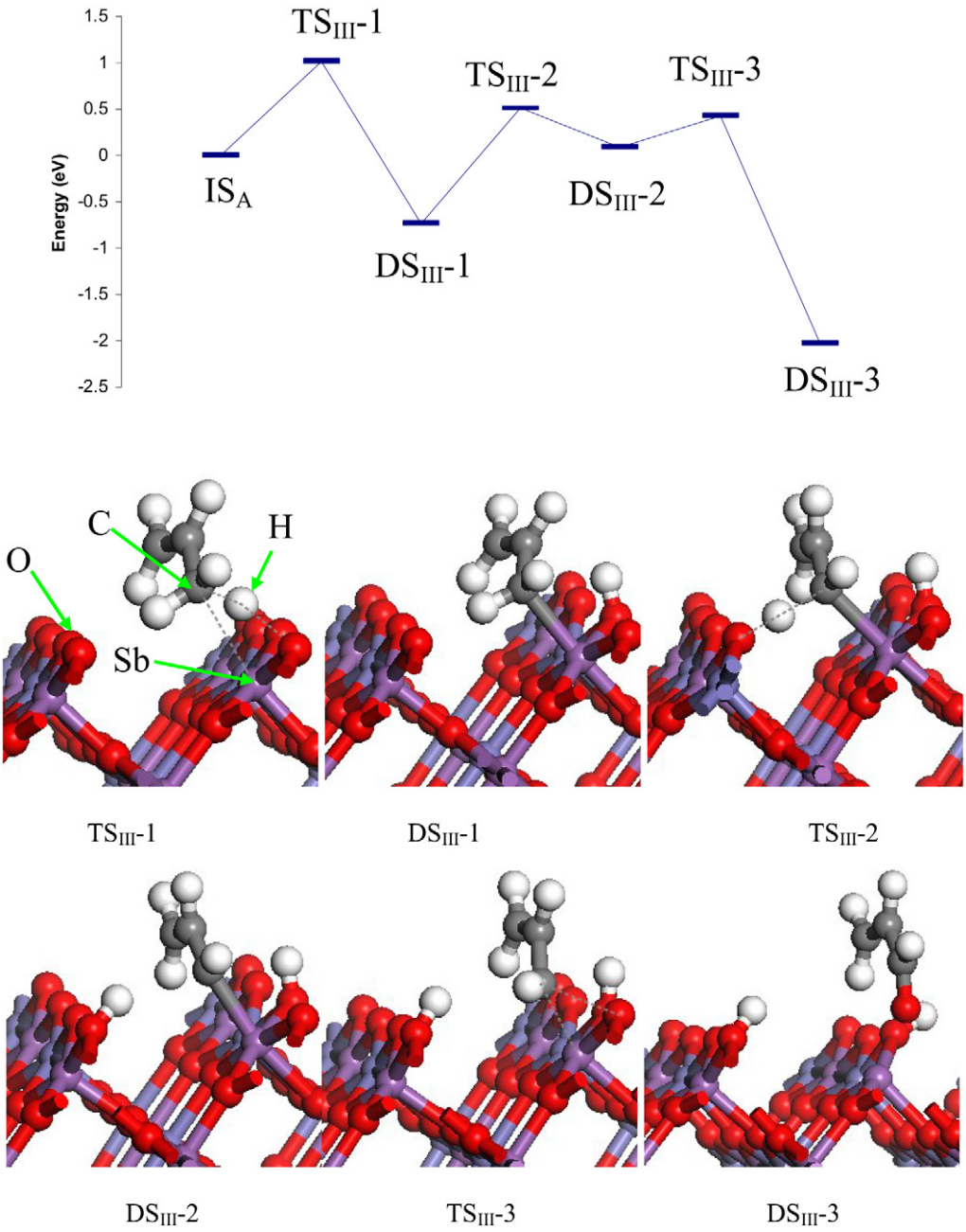

Fig. 6. Energy profile of path *III* for acrolein formation. The energy zero refers to the isolated systems (IS_A) in which propene is initially not in close contact with the surface (i.e. configuration *d* in Fig. 2).

mation of acrolein. This process is substantially exothermic (by 2.1 eV), with a small barrier of 0.42 eV. In the final configuration (DS_{III}-3), acrolein interacts weakly with the surface; the O-metal distances are >2.60 Å, indicating that the molecule can readily desorb.

Considering next the reaction that starts from the homolytic splitting (i.e., path *IV* in Fig. 7), we choose a different initial state (IS_B) in which propene interacts with the surface mainly via one allylic H atom [40]. Compared with IS_A in the heterolytic splitting path, the H···O distance in IS_B is relatively short (∼2.3 Å), indicating that the H atom is somewhat activated by the BO beneath. IS_B is also slightly less stable (by ∼0.06 eV) than IS_A. The barrier for the abstraction of the allylic H is relatively small (0.67 eV). In the TS (i.e. TS_{IV}-1), the C–H and O–H distances are 1.32 and 1.31 Å, respectively. Moreover, because of the H abstraction, the original CH_2 species of the molecule moves closer to a BO (3.10 Å), which neighbors, along [001], the BO responsible for the H abstraction. This abstraction leads to the formation of a π-allyl species (DS_{IV}-1) that attaches to both the dissociated H atom (2.11 Å) and a BO (2.76 Å). This step is then followed by C–O bond formation. The TS (TS_{IV}-2) forms when the C–O and H–O distances are 2.31 and 2.27 Å, respectively, and a small barrier of 0.16 eV is found. Because of the strong C–O bonding, this process is significantly exothermic by 1.56 eV. The resulting configuration (DS_{IV}-2) is very similar to DS_I-2 in path *I* or DS_{II}-2 in path *II* (i.e., the π-allyl binding to a BO); therefore, it is not surprising that the kinetics of the abstraction of the second H atom from DS_{IV}-2 also is similar to that of the abstraction of the second H in path *I* or *II*. A 1.35-eV barrier is calculated for H abstraction towards an adjacent BO along [010] in DS_{IV}-2, as shown in Fig. 7; the barrier for the H abstrac-

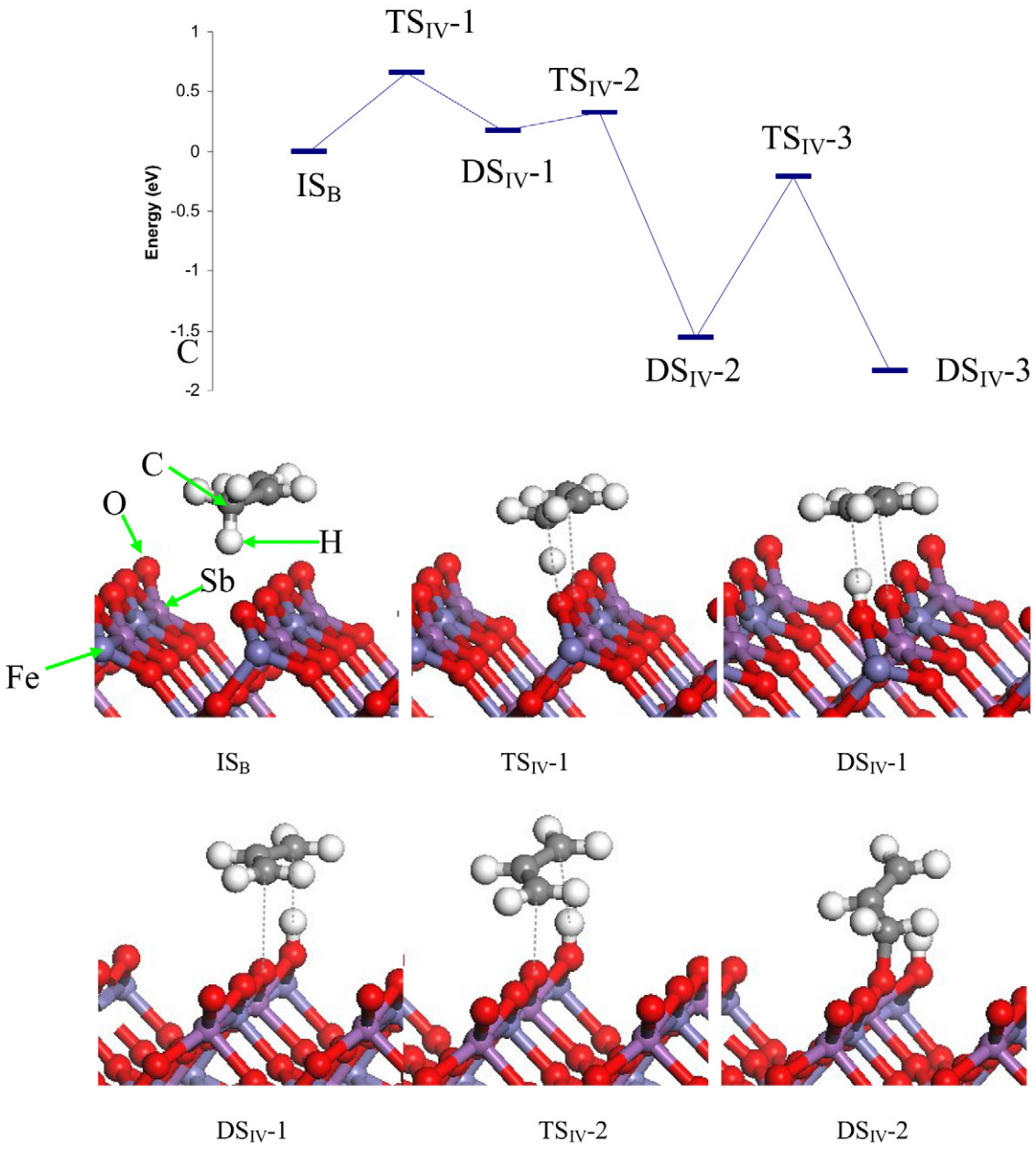

Fig. 7. Energy profile of path *IV* for acrolein formation. The energy zero refers to the isolated systems (IS_B) in which propene is initially not in close contact with the surface. The configurations involved in the abstraction of the second H atom (i.e. TS_{IV}-3 and DS_{IV}-3) are very similar to those in path *I* (i.e. TS_I-2 and DS_I-3 in Fig. 4), and thus are not shown. For better viewing, DS_{IV}-1 is shown from two different angles.

tion towards an Sb would also be expected to be similar to the corresponding value in path *II*.

4. Discussion

Based on the energy profiles of the paths described above, we see that in paths *I* and *II*, the energy barriers are close to the initial binding energy of the propene molecule. This suggests that desorption of the molecule can be competitive with oxidation via these paths, raising the issue of whether oxidation could result from direct dissociation of the molecule without the need to proceed through the chemisorbed precursor (i.e., paths *III* and *IV*). But significant barriers are identified in paths *III* and *IV*. Because the initial states in paths *III* and *IV* are already 1.25 eV higher than those in paths *I* and *II*, the oxidation via paths *III* and *IV* would be much more kinetically unfavorable; thus, in what follows, we discuss only paths *I* and *II* with the relevant experimental results.

Paths *I* and *II* have similar energy barriers, suggesting that both could be viable in forming acrolein. In path *I*, and even more so in path *II*, the abstractions of the first H (i.e., allylic H) and the second H have almost equal barriers, suggesting that both abstractions could be rate-determining. Experimentally, both the first and the second H abstractions have been proposed to be the rate-determining step [7,9], and O addition also was considered to be rate-determining by Allen et al. [10]. From our calculations, however, we clearly see that in paths *I* and *II*, propene initially chemisorbs on the surface, with the C–O bond already formed, and that after abstraction of the two Hs, it takes only an energy of $<\sim$0.3 eV to break the O-metal bonds (i.e., acrolein desorption). Therefore, we suggest that the inconsistency with experiment may be due to the difficulty in differentiating O addition and H abstraction experimentally [10]; as long as H abstraction (the rate-determining step) can be triggered, O addition also could occur readily under the same reaction conditions. Another inter-

esting observation of Allen et al. [10] is that under reaction conditions, propene can adsorb in a weakly held state, attributed to the adsorption–desorption equilibrium. This is consistent with our findings; due to the comparable binding energies of propene molecules and the oxidation barrier, desorption can be expected to occur before or during oxidation.

Our findings also may provide some insight into the mechanisms of propane oxidation, for which two possible routes have been proposed: the one-stage and two-stage routes, referring, respectively, to the direct conversion of propane to acrolein and the two-step conversion consisting of dehydrogenation of propane to propene and propene oxidation. In recent work [17], we identified the one-stage route. The reaction is triggered by the first H abstraction via a heterolytic splitting of a CH_3 species, followed by six more consecutive elementary steps. The largest barriers were calculated as ∼1.2 eV, corresponding to different C–H bond splittings. We also evaluated propene formation and found a similar barrier height for the initial dehydrogenation of propane. The similar barriers in the two processes is consistent with the experimental study of Bowker et al. [41], who observed the formation of propene and acrolein at the same temperature on $FeSbO_4$. In the current work, the barriers in propene oxidation are also very close to those in propene formation and the one-stage route of acrolein formation; that is, the one-stage and two-stage routes have comparable barriers. Thus, we suggest that both the one-stage and two-stage routes can contribute to acrolein formation.

We note that our study of propene oxidation refers to a clean surface and not to a partially hydroxylated surface, which may be a more likely situation after the dehydrogenation of propane. Nonetheless, our calculations show that the propene intermediate formed after the dehydrogenation of propane is not chemisorbed, because the dissociated H atom from propane binds to the bridging O and consequently hinders C–O bond formation. Thus, the propene intermediate can readily diffuse to clean surface sites, where the molecule can be chemisorbed, which are essentially the scenarios that we simulate in paths *I* and *II*. We also should note that, although we chose a well-defined $FeSbO_4$ surface with atomic ratio of Sb:Fe = 1:1 for this study, the actual catalyst working surface can be considerably more complicated (with, e.g., different Sb:Fe ratios or even different surface terminations), and oxygen vacancies exist [41]. Thus, further studies on these aspects are desirable. Finally, we note that our analysis is based on the energy barrier alone, whereas reaction kinetics depends on many other factors. Thus, microkinetic modeling may be able to provide more realistic information, such as the dominant path and the rate-determining step.

5. Conclusion

To summarize, we have investigated the most representative paths for propene oxidation to acrolein. We have found that the most favorable paths start from a chemisorbed state, and that acrolein formation is triggered by abstraction of an allylic H atom, followed by abstraction of a second H atom and finally desorption of acrolein. The oxidation path starting with a direct dissociation from a weakly physisorbed species has significantly higher barriers and thus is kinetically hindered. Compared with experimental results, our findings reconcile some differences in the mechanisms proposed previously. Furthermore, the barriers in propene oxidation are similar to those in the one-stage route for propane oxidation, suggesting that the two-stage route also can contribute to acrolein formation in propane oxidation. We note that both this and our previous study have concentrated on mechanisms on the perfect surface with a stoichiometric ratio of Sb:Fe. Future work will explore the catalytic processes on different surfaces, especially those with oxygen vacancies.

Acknowledgments

This work was funded by the EPSRC Portfolio Partnership Project on Synthesis and Design of Functional Materials (EP/D504872). The authors are grateful for an allocation of computer time on the HPCx through the Material Chemistry Consortium, also funded by the Portfolio Partnership.

References

[1] R.K. Grasselli, J.D. Burrington, Adv. Catal. 30 (1981) 133.
[2] R.K. Grasselli, Top. Catal. 21 (2002) 79.
[3] V. Fattore, Z.A. Fuhrman, G. Manara, B. Notari, J. Catal. 37 (1975) 223.
[4] I. Aso, T. Amamoto, N. Yamazoe, T. Seiyama, Chem. Lett. (1980) 365.
[5] N. Burriesci, F. Garbassi, M. Petrera, G. Petrini, J. Chem. Soc. Faraday Trans. 78 (1982) 817.
[6] Z. Dziewiecki, A. Makowski, React. Kinet. Catal. Lett. 1 (1980) 51.
[7] J.D. Burrington, C.T. Kartisek, R.K. Grasselli, J. Catal. 87 (1984) 363.
[8] I. Aso, S. Furukawa, N. Yamazoe, T. Seiyama, J. Catal. 64 (1980) 29.
[9] G.W. Keulks, M. Lo, J. Phys. Chem. 90 (1986) 4768.
[10] M. Allen, R. Betteley, M. Bowker, G.J. Hutchings, Catal. Today 9 (1991) 97.
[11] R.K. Grasselli, D.D. Suresh, J. Catal. 25 (1972) 273.
[12] E. Van Steen, M. Schnobel, R. Walsh, T. Riedel, Appl. Catal. A: Gen. 165 (1997) 349.
[13] S. Albonetti, F. Cavani, F. Trifirò, Catal. Rev. Sci. Eng. 38 (1996) 413.
[14] R.K. Grasselli, Catal. Today 49 (1999) 141.
[15] M.M. Lin, Appl. Catal. A: Gen. 207 (2001) 1.
[16] M.O. Guerrero-Pérez, J.N. Al-Saeedi, V.V. Giulants, M.A. Bañares, Appl. Catal. A: Gen. 260 (2004) 93.
[17] C. Zhang, C.R.A. Catlow, J. Phys. Chem. C 112 (2008) 9783.
[18] G. Centi, R.K. Grasselli, F. Trifirò, Catal. Today 13 (1992) 661.
[19] P. Berlepsch, T. Armbruster, J. Brugger, A.E. Criddle, S. Graeser, Mineral. Mag. 67 (2003) 31.
[20] R. Grau-Crespo, N.H. de Leeuw, C.R.A. Catlow, J. Mater. Chem. 13 (2003) 2848.
[21] R. Grau-Crespo, N.H. de Leeuw, C.R.A. Catlow, Chem. Mater. 16 (2004) 1954.
[22] R. Grau-Crespo, F. Cora, A.A. Sokol, N.H. de Leeuw, C.R.A. Catlow, Phys. Rev. B 73 (2006) 035116.
[23] R. Grau-Crespo, C.R.A. Catlow, N.H. de Leeuw, J. Catal. 248 (2007) 77.
[24] X. Obradors, J. Bassas, J. Rodriguez, J. Pannetier, A. Labarta, J. Tejada, F.J. Berry, J. Phys.: Condens. Matter 2 (1990) 6801.
[25] P. Berlepsch, J. Brugger, Schweizer Strahler 11 (1999) 425.
[26] G. Kresse, J. Furthmuller, Comput. Mater. Sci. 6 (1996) 15.
[27] G. Kresse, J. Furthmuller, Phys. Rev. B 54 (1996) 11169.
[28] G. Kresse, J. Hafner, Phys. Rev. B 48 (1993) 13115.
[29] G. Kresse, J. Hafner, J. Phys.: Condens. Matter 6 (1994) 8245.
[30] V.I. Anisimov, J. Zaanen, O.K. Andersen, Phys. Rev. B 44 (1991) 943.
[31] A. Rohrbach, J. Hafner, G. Kresse, J. Phys.: Condens. Matter 15 (2003) 979.
[32] A.I. Liechtenstein, V.I. Anisimov, J. Zaanen, Phys. Rev. B 52 (1995) R5467.
[33] S.L. Dudarev, G.A. Botton, S.Y. Savrasov, C.J. Humphreys, A.P. Sutton, Phys. Rev. B 57 (1998) 1505.
[34] J.P. Perdew, A. Zunger, Phys. Rev. B 23 (1981) 5048.
[35] S.H. Vosko, L. Wilk, M. Nusair, Can. J. Phys. 58 (1980) 1200.
[36] J.P. Perdew, J.A. Chevary, S.H. Vosko, K.A. Jackson, M.R. Pederson, D.J. Singh, C. Fiolhais, Phys. Rev. B 46 (1992) 6671.
[37] A. Rohrbach, J. Hafner, G. Kresse, J. Phys.: Condens. Matter 15 (2003) 979.
[38] G. Kresse, D. Joubert, Phys. Rev. B 59 (1999) 1758.
[39] G. Henkelman, B.P. Uberuaga, H. Jónsson, J. Chem. Phys. 113 (2000) 9901.
[40] There exist other possible homolytic paths. For example, when the reaction starts from an initial state, in which the C of the CH_3 species is directly above a BO, it would proceed via a C–H–O three-centered TS and end with a configuration in which the BO binds to both the dissociated H atom and the C atom. Because the resulting configuration is much less stable than that shown in path *IV*, we omit this possibility.
[41] M. Bowker, C.R. Bicknell, P. Kerwin, Appl. Catal. A: Gen. 136 (1996) 205.